Scattering Patterns of Multiply Continuous Cubic Phases in Block Copolymers. I. The Model

Piotr Garstecki[†,‡] and Robert Hołyst[*,†,§]

Institute of Physical Chemistry PAS Department III, Kasprzaka 44/52, 01-224 Warsaw, Poland, and Cardinal Stefan Wyszyński University, WMP-SNS, Dewajtis 5, Warsaw, Poland

ABSTRACT: The X-ray scattering amplitudes are given for the multicontinuous P, D, G, and I-WP cubic phases formed in block copolymer systems. The formulas can be used to retrieve the scattering amplitudes for an arbitrary n-block copolymer system adopting one of the above multiply continuous triply periodic structures (MCTPS).

1. Introduction Surfaces in Copolymer Systems

An A−B diblock copolymer is a polymer consisting of a sequence of A-type monomers covalently joined to a sequence of B-type monomers. Even a small incompatibility (difference in interactions) between monomers A and B can induce a strong tendency toward separation. However given that A- and B-homopolymers are covalently joined in a diblock, the system cannot undergo a macroscopic phase separation. Instead a number of order−disorder phase transitions take place in the system between the isotropic phase and spatially ordered phases. In an ordered phase the A-rich and B-rich domains, roughly of the size of a the particular block's radius of gyration, are arranged periodically in one, two, or complex three-dimensional structures. The covalent bond joining the blocks rests at the interface between the A and B-rich domains.[1] These interfaces are the internal surfaces inside the block copolymer structure and can be modeled as planar sheets, cylinders, spheres or, in the case of MCTPS, by triply periodic surfaces.

At the mesoscopic level of description the Landau-Ginzburg model of the phase transitions in diblock copolymer system was formulated by Leibler[2] and later refined by Fredrickson et al.[3] Matsen et al.[4−6] applied the self-consistent field theory to the phase transitions in this system. For $\phi_A = 0.5$ (ϕ_A is the volume fraction of A monomers in the system) only the lamellar phase is stable with periodic stack of flat interfaces. As we decrease ϕ_A the double gyroid phase appears. This phase consists of two gyroid surfaces in a unit cell. They form boundaries between A-rich and B-rich domains. The phase has $Ia\bar{3}d$ symmetry[7] and each surface has genus 5 per unit cell.[7,8] Upon further decrease of the concentration of one of the components a transition to the hexagonal phase and bcc phase is observed. In the hexagonal phase a minority component forms cylinders arranged on the hexagonal lattice and inserted in the matrix of the majority component. In the bcc phase (symmetry $Im\bar{3}m$) the minority component forms spheres arranged on the bcc lattice and surrounded by the majority component. The last phase which appears in the system is the CPS[9] (closed-packed spheres) phase. It consists of the spheres of the minority phase arranged either on the fcc or hcp lattice. The theoretical studies of the system were greatly stimulated by experiments. The cylindrical, spherical and lamellar phases have been known for a long time,[10] but only recently the novel bicontinuous structures have been discovered in the diblock copolymer systems.[11−13] The originally discovered bicontinuous ordered structure has been misidentified in the TEM experiments;[13] later it has been shown that this structure is the double gyroid phase.[14] The first observation and identification of the gyroid phase in block copolymers was done almost simultaneously by Hajduk et al.[15] and Schulz et al.[16]

One of the common techniques used to identify the ordered phases in block copolymers is the small-angle X-ray scattering (SAXS). The literature on this subject is vast, let us cite some recent ones.[17−25] One of the problems encountered in the identification of the architecture of the ordered multicontinuous structures is the lack of simple analytical expressions for the X-ray scattering amplitudes. The symmetry of the structure can be identified on the basis of the relative positions of the Bragg peaks but the internal architecture of the structure can only be resolved in a quantitative analysis of the scattering intensities.

It is the purpose of this paper to provide analytical expressions for the X-ray scattering amplitudes in an n-block copolymer system for gyroid (G)[26] simple cubic (P),[27] double diamond (D) and wrapped package (I-WP) structures. These formulas are simple enough to allow the fitting to the experimental spectra in the standard spread-sheet program without heavy computer simulations. In particular, the following information can be derived: (i) the type of the structure, (ii) number of channels in a structure, (iii) size of a channel occupied by any block and consequently the radius of gyration for this block, and (iv) the width of the interface between different channels.

The paper is organized as follows: the next section introduces the basic concepts needed to study the multiply continuous triply periodic structures (MCTPS) in block copolymer systems. In section 3, we derive the formulas for the scattering amplitudes. Next the numerical results are described (sections 4 and 5). Finally, we give a general solution (section 6) for the amplitudes and introduce the widths of the interfaces into equations (section 7).

* To whom correspondence should be addressed.
† Institute of Physical Chemistry PAS Department III.
‡ Present address: Chemistry & Chemical Biology Department, Harvard University, 12 Oxford St., Cambridge, Ma 02138, USA. E-mail: pgarstecki@gmwgroup.harvard.edu.
§ Cardinal Stefan Wyszyński University.
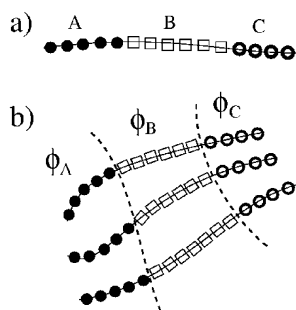
Figure 1. (a) Schematic illustration of a triblock copolymer molecule. Monomers A, B, and C form subsegments of the whole chain. The blocks are covalently bonded, and it is through these points that the interface between spatially separated domains run (b).

2. Geometry of the MCTPS

2.1. *n*-Block Copolymer Molecule. The block copolymer molecule is formed by a linear sequence of covalently bond homopolymer chains. Each of the homopolymer chains (blocks) is composed of one type of monomers. The blocks are characterized by the chemistry of the monomers and by the degree of polymerization N_i, where i refers to the number of the block in the sequence. A schematic representation of a triblock copolymer molecule is given in Figure 1a. The volume fraction ϕ_i of each of the blocks can be calculated through:

$$\phi_i = \frac{N_i v_i}{\sum_{j=1}^{n} N_j v_j} \tag{1}$$

where v_i is a volume of a single monomer of the ith block and n is the number of blocks. Because of both the entropic and energetic interactions the blocks constituted of different types of monomers have a tendency to spatially separate. Below a certain transition temperature, this tendency wins over mixing, and the blocks locally segregate. Blocks of the same type are driven close to each other and form distinct subvolumes in which their concentration is higher than in the rest of the system. The volume fractions of these domains correspond to the volume fractions of each of the blocks. The interfaces between these separate volumes occupied by different blocks run through the points on the molecule at which the chemical bonds between the subsequent blocks are positioned (see Figure 1b). The bonds keeping the blocks together set up strong geometrical constrains on the morphology of the resulting phase. Namely the volume fractions of each of the block have to be preserved locally and thus the typical diameters of the volumes occupied by different blocks have to be on the order of the given block's radius of gyration.

2.2. The Ordered Phases. The phase diagrams of *n*-block copolymer systems have been extensively studied both experimentally and theoretically. The variety of possible phases and geometrical arrangements of the subvolumes associated with different blocks grows very fast with the number of blocks. The simplest case on which the reader can gain some intuition about the potential morphologies is a diblock copolymer system. Even such a relatively simple system offers quite a rich variety of the possible phases. There are three general

criteria by which the phases can be distinguished: (1) the spatial continuity of the domains, (2) dimensionality, and (3) order−symmetry of the subvolumes. The first criterion is associated strongly with the volume fractions of each of the blocks. In case of a *di*-block system there are only two subvolumes ϕ_1 and $\phi_2 = 1 - \phi_1$. If there is a strong asymmetry in the values of the volume fractions the spaces occupied by the minority block will be discontinuous—they will form either spherical or almost spherical closed subspaces saturated in the continuous matrix of the majority component. On the other hand when the volume fractions are comparable both of the resulting domains will be continuous—they will span the whole system in at least one direction. Although being only a very rough guide, the same heuristics will apply to the systems of multiblock copolymers.

Another feature of the separated polymer domains is their dimensionality. The discontinuous−micellar domains are not elongated in any dimension. Giving the domains the freedom to extend in one or two dimensions, one obtains a notion of the cylinders (1D) or layers (2D). It should be thought of as a local description. The cylinders rich in one of the blocks can join at different coordination numbers and form a higher dimensional network. Still its local morphology is one-dimensional. Similarly the two-dimensional layerlike domains need not to be planar. They can merge through the so-called passages resulting in a structure which is continuous in all of the three directions.

Finally in a certain range of the parameters, the system can exhibit three basic types of the translational order. The simplest example is a lamellar system in which the planar layers containing each of the blocks are stacked one on each other. Since the domains are extended in two directions there is only one dimension left to exhibit order. The cylinders can form an ordered two-dimensional hexagonal lattice perpendicular to their direction of continuity. Finally, the micells can be arranged on a three-dimensional regular lattice. As was mentioned before, such a system is composed of the discontinuous domains saturated in a triply continuous matrix. This article deals with yet another kind of structures in which all of the domains are continuous and the whole system exhibits a full three-dimensional order. Such architectures can be physically realized by either continuous networks of connected cylinders or by curved triply periodic layers.

In case of the micellar domains the interfaces running through the bonds between subsequent blocks resemble spheres. For the hexagonal phase the interfaces are cylindrical and for the lamellar layers the interfaces are flat. When there is a three-dimensional order and all of the domains are continuous, the interfaces can be approximated by the constant mean curvature (CMC)[28] or parallel[29] triply periodic surfaces (TPS). The parallel surfaces (PS) can be derived from the triply periodic minimal surfaces (TPMS)[30] (see Figure 3). The TPMS is a CMC surface with the mean curvature equal to zero at every point on the surface. PS (or CMC) divide the space into two distinct, nonintersecting subvolumes or channels. Each of the channels forms a triply periodic network. An *n*-domain *n*-continuous cubic structure can be modeled by a set of $n - 1$ TPSs (interfaces).

It is a subject of an ongoing dispute whether it is the CMC or PS families that better describe the block copolymer cubic phases.[32] As it has been argued[29,33,34] the PS are very close to the cmc surfaces and both
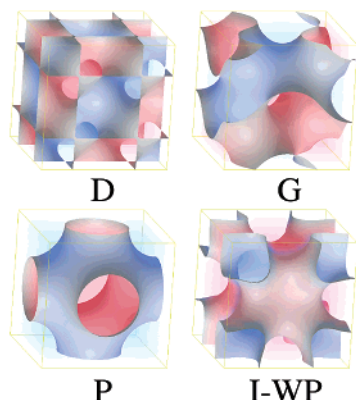
Figure 2. Unit cells of the triply periodic minimal surfaces studied in this work.

solutions provide a very close agreement between various calculated characteristics.[35-38] In our model, we have chosen to work with the PS.

Below we will discuss multiply continuous triply periodic structures (MCTPS).

2.3. A Basic Motif for the MCTPS—A Single Channel. The abstract template for the MCTPS are the TPMS. In this work, we have taken into account the four simplest[31] and most commonly known TPMS—Schoen's P (plumber's nightmare) surface, Schwartz's double diamond D surface, the G gyroid, and I-WP surfaces (see Figure 2). The P, D, and G TPMS are balanced—they divide the volume of the unit cell into two identical channels. Namely, one can move one of the resulting networks onto the other by a set of simple symmetry operations. The I-WP is not balanced—it divides the volume into two different networks of cylinders. Although both of them belong to the same symmetry group, one of them has four coordinated nodes and the other is eight coordinated. The lack of translational symmetry between the two networks introduces additional free parameter which has to be taken into account when resolving the structure of a given *n*-block copolymer system. This problem will be addressed in detail in the subsection containing the results for the I-WP based channels and in the following article dealing with the application of our model to the analysis of the experimental scattering spectra.

To distinguish between the two channels created by the TPMS the surface has to be oriented. One can imagine that one of the channels has been filled with *white* paint while the other with a *black* one. Then the surface is white on one of its sides and black on the other. Now, at every point on the minimal surface, we can draw an axis ξ that would be normal to it. We can set the origin on the TPMS and direct the ξ axis into the white channel. Then ξ would acquire negative values in the black domain and positive in the white one.

A parallel surface is created by shifting the interface by a constant displacement ξ_1. The TPMS is itself a special case of a PS with $\xi_1 = 0$. Now if we shift the surface to lower (negative) values of ξ the black channel will shrink and the white channel will be expanded (see Figure 3). The volume fraction occupied by the black channel $\{V_{\text{black}}: \xi(\mathbf{r}) < \xi_1\}$ can be expressed[39] as a function of the normalized displacement $\xi_1^* = \xi_1/a$ (where a is the lattice parameter of the unit cell):

$$\phi_1(\xi_1^*) = \phi_- + s_0^* \xi_1^* + \frac{2}{3}\pi\chi\xi_1^{*3} \tag{2}$$
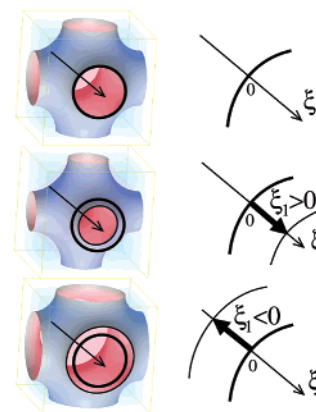
Figure 3. Schematic illustration of the construction of the parallel surfaces (PS). At each point on the TPMS an axis ξ normal to it is drawn. It is invariably pointed into one of the channels (here marked by red) into which the TPMS divides the volume. A PS can be obtained by spanning a surface through all of the points on the axes ξ of the same value of the displacement ξ_1.

Table 1. Characteristics of the P, D, G, and I-WP Triply Periodic Minimal Surfaces[a]

TPMS	χ	s_0^*	ϕ_-	β
P	−4	2.3458	0.5	3.18
D	−16	3.8384	0.5	1.47
G	−8	3.0966	0.5	1.64
I−WP	−12	3.5543	0.477	1.42

[a] χ is the Euler characteristic per unit cell, s_0^* is the normalized surface area per unit cell, and ϕ_- is the volume fraction of the channel corresponding to the negative values of the displacement from the base TPMS (see text for explanation). The β parameter allows a reconstruction of the displacement ξ of the parallel surface boundary of the network occupying volume fraction ϕ (see eq 3).
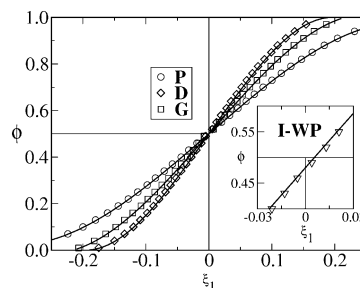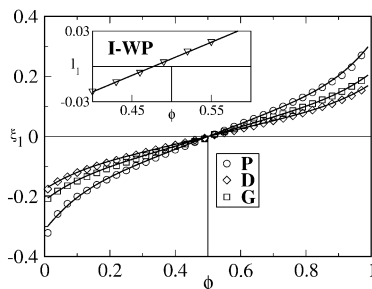

Figure 4. Volume fraction of the black channel given by the condition $\xi(\mathbf{r}) < \xi_1$ as a function of the displacement ξ_1 for the P, D, and G TPMS. The circles (P), diamonds (D), and squares (G) give the numerical results while the solid lines present the analytical approximation (eq 2). The inset underlines the fact that the I-WP TPMS is not balanced. The volume fraction of the four coordinated black channel associated with the negative values of ξ is equal to 0.477.

Here ϕ_- is the volume fraction of the black channel determined by the base TPMS $\{\mathbf{r}: \xi(\mathbf{r}) < 0\}$ ($\phi_- = 0.5$ for P, D, G and 0.477 for I-WP), s_0^* is the normalized surface area of the base TPMS ($s_0^* = s_0/a^2$) and χ is the Euler characteristic of the base TPMS. The values of the normalized surfaces and the Euler characteristics for the P, D, G, and I-WP TPMS are given in Table 1. As is shown in Figure 4 the volume fraction ϕ of the black channel is smaller than 0.5 (0.477 for I-WP) for $\xi_1^* < 0$ and greater than this value for $\xi_1^* > 0$.

A single parallel surface structure can serve as a model for the unit cell of a separated diblock copolymer system with one of the blocks occupying the black and

Figure 5. Displacement ξ_1 of a PS as a function of the volume fraction ϕ of the inclosed network. The symbols show numerical results while the solid lines present the fits through eq 3.

the other the white channel. Knowing the molecular masses M_i of the constituting monomers and the degrees of polymerization N_i of each of the two blocks, one can calculate the corresponding volume fractions of the blocks through eq 1. Now we can find the position ξ_1 of a PS interface which divides the space into required fractions by inverting relation 2. It is a difficult task, since the volume fraction ϕ_1 (eq 2) is given by a third degree polynomial in ξ_1. It is easier to use the following approximation

$$\xi_1^*(\phi_1) = \frac{1}{s_0^*}(\phi_1 - \phi_-) + \beta(\phi_1 - \phi_-)^5 \qquad (3)$$

where β is a fitted parameter given in Table 1. The efficiency of the latter approximation is shown in Figure 5. Now the volume occupied by the first block is defined by

$$V_1 = \{\mathbf{r}: \ \xi(\mathbf{r}) < \xi_1\} \qquad (4)$$

where the modulus of the $\xi(\mathbf{r})$ is the distance to the base TPMS and it's sign is negative on the black and positive on the white side of the base TPMS.

In an *n-block* copolymer system, if the separated domains adopt a MCTPS the interfaces can also be modeled by a set of $n-1$ PS. To localize them in the terms of the displacement ξ, one has to use the summed volume fractions $\{\tilde{\phi}_i\}$

$$\tilde{\phi}_i = \sum_{j=1}^{i} \phi_i \qquad (5)$$

where ϕ_i are the volume fractions of the constituting blocks. The positions of the interfaces can be calculated through (3) as $\xi_i^*(\tilde{\phi}_i)$. The first interface is the boundary of the first channel for which $\tilde{\phi}_1 = \phi_1$. The next PS has to surround both the first channel and the layer of volume fraction ϕ_2 thus $\tilde{\phi}_2 = \phi_1 + \phi_2$ (see Figure 6). This procedure allows determination of all of the $(n-1)$ PS interfaces in terms of their displacement $\{\xi_i; \ i \in (1, n-1)\}$ from the base TPMS. The volumes occupied by each of the blocks are defined by

$$V_i = \{\mathbf{r}: \ \xi_{i-1} < \xi(\mathbf{r}) < \xi_i; \ i \in (1, n)\} \qquad (6)$$

where for conveniency the outermost values of the displacement are set to $\xi_0 = -\infty$ and $\xi_n = \infty$.

For the amplitude calculations we need the electron density distribution $\rho(\mathbf{r})$. It acquires a different value $\rho(\mathbf{r}) = \rho_i$ in each of the n domains:

$$\rho(\mathbf{r}) = \rho_i | \mathbf{r} \in V_i \qquad (7)$$
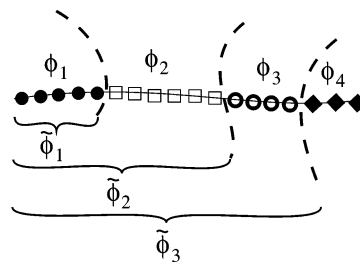
Figure 6. Recovery of the displacements ξ_i of the interface surfaces. To do this one has to use the summed volume fractions $\tilde{\phi}_i$. See text for explanation.
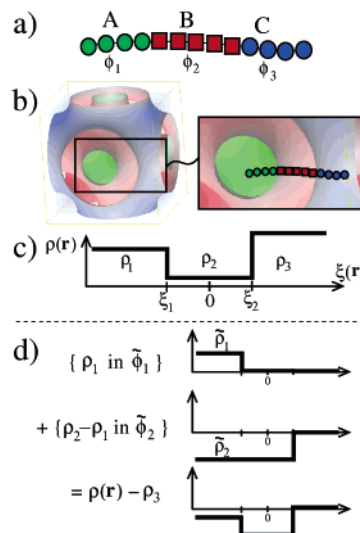
Figure 7. Schematic illustration of the triblock copolymer molecule (a), the resulting PS interfaces between the continuous domains rich in A (green), B (red) and C (blue) monomers (b) and a hypothetical electron density distribution in the direction ξ normal to the base TPMS (c). All of the data which will be reflected in the scattering pattern are contained in a shifted electron distribution which can be expressed as a sum of to distributions associated with single channels (d). See section 2.3 for a detailed explanation.

A schematic illustration of the electron density map for a triblock copolymer system is shown in Figure 7c. The relative amplitudes of different Bragg reflections depend only on the electron density contrast. Subtracting any constant from the electron density distribution $\rho(\mathbf{r})$ does not change the scattering pattern. For simplicity, we have chosen to subtract the density of the last channel ρ_n. Such a modified electron density map can be represented by the following sum (see Figure 7d)

$$\rho(\mathbf{r}) = \sum_{i=1}^{n-1} \tilde{\rho}_i(\mathbf{r}) \qquad (8)$$

where the electron densities $\{\tilde{\rho}_i(\mathbf{r}); \ i \in (1, n-1)\}$ are given by

$$\tilde{\rho}_i(\mathbf{r}) = \begin{cases} \rho_i - \rho_{i+1}; & \xi(\mathbf{r}) \leq \xi_i \\ 0 & \xi(\mathbf{r}) > \xi_i \end{cases} \qquad (9)$$

Any MCTPS electron density map $\{\phi_i, \rho_i\}$ can be built from a sum of single channels $\{\tilde{\phi}_i, \tilde{\rho}_i(\mathbf{r})\}$. This will greatly facilitate calculations of the scattering amplitudes.

3. The Scattering Amplitude

The scattering amplitude is a Fourier transform of the electron density within the unit cell:

$$A(\mathbf{q}, \rho(\mathbf{r})) = \int d\mathbf{r}\, \rho(\mathbf{r}) \exp[i\mathbf{q}\mathbf{r}] \qquad (10)$$

where $\mathbf{q} = (2\pi/a)[h, k, l]$ is the scattering wave vector. Inserting $\rho(\mathbf{r})$ from eq 8 we obtain

$$A(\mathbf{q}, \tilde{\phi}_1, \tilde{\rho}_1, \ldots \tilde{\phi}_{n-1}, \rho_{n-1}) = \sum_{i=1}^{n-1} \int \tilde{\rho}_i(\mathbf{r}) \exp[i\mathbf{q}\mathbf{r}] \quad (11)$$

Thus, we can express the scattering amplitude as a sum of $n - 1$ amplitudes arising from the consecutive channels:

$$A(\mathbf{q}, \rho(\mathbf{r})) = \sum_{i=1}^{n-1} A_i(\mathbf{q}, \tilde{\phi}_i, \rho_i) \qquad (12)$$

where since the density, ρ_i, is constant in the ith channel, we have

$$A_i(\mathbf{q}, \tilde{\phi}_i, \tilde{\rho}_i) = \tilde{\rho}_i \int_{\xi(\mathbf{r}) \leq \xi_i} d\mathbf{r} \exp[i\mathbf{q}\mathbf{r}] = \tilde{\rho}_i \mathscr{A}(\mathbf{q}, \xi_i) \quad (13)$$

The last expression $\mathscr{A}(\mathbf{q}, \xi)$ is a Fourier transform of a single channel occupying a volume fraction $\phi(\xi)$ (eq 2) with a uniform electron density equal to unity. Besides the scattering vector $\mathbf{q}$, it depends only on the volume fraction of the channel or equivalently on the displacement ξ of it's interface PS. Thus, to retrieve a set of scattering amplitudes for any postulated MCTPS architecture, we only need to know how $\mathscr{A}$ depends on ξ.

In general $\mathscr{A}$ is a functional of a geometrically complex condition $\xi(\mathbf{r}) \leq \xi$. It is the object of this work to substitute such a three-dimensional Fourier transform by a simple formula. As in the case of the already published[36,37] results for the bicontinuous cubic phases formed in amphiphilic mixtures the scattering amplitude for the basic motif can be expressed by

$$\mathscr{A}(\mathbf{q}, \xi) = \int_{\xi(\mathbf{r}) \leq \xi} d\mathbf{r} \exp[i\mathbf{q}\mathbf{r}] = \mathscr{F}^S(\mathbf{q})\mathscr{F}^M(\mathbf{q}, \xi) \quad (14)$$

where $\mathscr{F}^S$ is a structure factor (SF) associated with the base TPMS and all of the dependence on the volume fraction is contained in the molecular factor (MF) $\mathscr{F}^M$. As it will be shown in detail in the following section the MF can be very well approximated by

$$\mathscr{F}^M(\mathbf{q}, \xi) =$$
$$\begin{cases} \sin(q\alpha_{hkl}\xi)/q\alpha_{hkl}| & hkl \text{ allowed by symmetry of TPMS} \\ \cos(q\alpha_{hkl}\xi)| & hkl \text{ allowed only by symmetry} \\ & \text{of networks} \end{cases}$$
$$(15)$$

The 2-fold nature of the MF arises from the difference in the symmetry of the base TPMS and the channel interfaces given by parallel surfaces. In a case of all of the balanced TPMS the minimal surface belongs to a higher symmetry group than the parallel surfaces. Higher symmetry sets more rigorous restrictions on the allowed hkl combinations. Thus, some of the Bragg reflections of a MCTPS are allowed both by the TPMS symmetry group and by the symmetry of the networks, and some of the peaks are allowed only by the lower

symmetry of the channels. This natural distinction in the form of the MF leads to an excellent agreement with the model proposed for the bicontinuous cubic phases. Namely, inserting an electron density distribution $\rho(\xi)$ which is symmetric with respect to the base minimal surface ($\xi = 0$) causes the amplitudes given by a symmetric MF to cancel each other which is in agreement with the reflection conditions set by the symmetry of the TPMS.

To check the latter proposal (eq 15) of an analytical expression for the scattering amplitudes we have performed numerical calculations. The unit cells of the P, D, G and I-WP TPMS[30] have been projected on a cubic grid $N_{grid} \times N_{grid} \times N_{grid}$ of the maximum size $N_{grid} = 128$ and triangulated. Then at each point $\mathbf{r}_{ijk}$ on the grid the distance $d(\mathbf{r}_{ijk})$ to the base TPMS has been calculated and assigned a positive sign on one side of the base TPMS surface and negative on the other. Given such a distance map the integral eq 14 has been evaluated as

$$\mathscr{A}^{num}(\mathbf{q}, \xi) = \frac{1}{N_{grid}^3} \sum_{i,j,k=1}^{N_{grid}} \Theta(\xi - d(\mathbf{r}_{ijk})) \exp[i\mathbf{q}\mathbf{r}_{ijk}]$$
$$(16)$$

where $\Theta(x)$ is a Heaviside step function ($\Theta(x) = 0$ for $x < 0$ and 1 for $x \geq 0$).

For the first group of peaks (allowed by the TPMS symmetry) the SFs have been established previously[36,40,41] as a Fourier transform of the base minimal surface within the unit cell:

$$\mathscr{F}^S = \int_{TPMS} d^2r \exp[i\mathbf{q}\mathbf{r}] \qquad (17)$$

For the other reflections the SFs are simply the values of the amplitudes (eq 16) for $\xi = 0$.

The following subsections contain a detailed description of the fitting results for the P, D, G, and I-WP TPMS based phases. Also the data needed to reconstruct the scattering patterns for an arbitrary multicontinuous cubic phase are given for the most prominent reflections. To enter the list each peak had to be among the 15 strongest reflections for any volume fraction of the channel $\phi \in (0.2, 0.8)$. Both mono crystalline and powder samples (including a multiplicity factor) spectra have been taken into account. Therefore, the list guarantees that in either case the 15 highest intensity peaks are included.

4. Results for the Balanced TPMS

4.1. The Schoen P Surface. The P—also called plumber's nightmare—surface (Figure 2) belongs to an $Im\bar{3}m$ symmetry group. It sets up the following reflection conditions:[42]

$$Im\bar{3}m: \begin{cases} hkl: & h + k + l = 2n \\ 0kl: & k + l = 2n \\ hhl: & l = 2n \\ h00: & h = 2n \end{cases} \qquad (18)$$

with all of the hkl Miller indices permutable. The symmetry group of the network is $Pm\bar{3}m$, and it does not restrict any combination of the hkl indices. Since both groups are centrosymmetric, it is possible to set the origin in such a way as to make all of the scattering amplitudes real. As in the case of all four of the explored
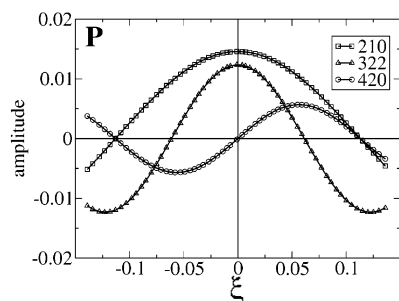
Figure 8. Amplitudes for the 210, 322, and 420 Bragg reflection arising from a single channel bounded by a PS derived from a P TPMS. The 420 reflection is allowed by the symmetry group of the TPMS ($Im\bar{3}m$) and exhibits an anti-symmetric (sine) form of the MF while the peaks allowed only by the lower symmetry group of the networks ($Pm\bar{3}m$)—210 and 322—have the symmetric cosine form (see eq 15). The symbols show the numerical results while the solid lines present the fit through eq 15.

Table 2. Scattering Data for the P TPMS Based Multicontinuous Cubic Phases[a]

The Scattering Data for the **P** Multicontinuous Cubic Phases

hkl	M_{hkl}	F^S_{hkl}	F^M	α_{hkl}	hkl	M_{hkl}	$F^S_{hkl}F^M$		α_{hkl}
0 0 0	1	0.5	ϕ		3 3 0	12	0.2155	s	1
1 0 0	6	−0.1651	c	0.97	4 2 0	24	0.1580	s	1
1 1 0	12	−0.4496	s	1.14	4 2 1	48	0.0045	c	1
1 1 1	8	0.0594	c	0.96	3 3 2	24	0.2795	s	1
2 0 0	6	−0.5444	s	1	4 2 2	24	0.2536	s	1
2 1 0	24	0.0146	c	1	4 3 0	24	−0.0062	c	1
2 1 1	24	0.4565	s	1.03	5 0 0	6	−0.0057	c	1
2 2 1	24	−0.0182	c	0.97	3 3 3	8	−0.0093	c	1
3 0 0	6	0.0180	c	0.98	5 1 1	24	0.0056	c	1
3 1 0	24	0.0985	s	1	4 3 2	48	−0.0058	c	1
3 1 1	24	−0.0152	c	0.97	5 2 2	24	−0.0053	c	1
2 2 2	8	−0.4056	s	1	4 3 3	24	−0.2680	s	1
3 2 0	24	0.0057	c	0.93	5 3 2	48	−0.1356	s	1
3 2 1	48	−0.2177	s	1	4 4 3	24	0.0057	c	1
4 0 0	6	0.2454	s	1	5 3 3	24	0.0050	c	1
3 2 2	24	0.0123	c	1	4 4 4	8	0.2597	s	1
4 1 1	24	−0.2425	s	1	5 4 3	48	0.1795	s	1

[a] For each *hkl* reflection the multiplicity factor $\mathscr{M}_{hkl}$, the structure factor $\mathscr{F}^S_{hkl}$, the form of the molecular factor $\mathscr{F}^M$ and the α_{hkl} correction parameter is given. "s" stands for the sine function and "c" for the cosine (eq 15). See text for explanation.

TPMS, we have chosen a phasing for which the amplitude of the 000 reflection is normalized to the volume fraction of the network:

$$\mathscr{A}(\mathbf{q} = 0, \xi) = \tilde{\phi}(\xi) \qquad (19)$$

This results in the same values of the SF's as for the bicontinuous cubic phases[36] in which the 000 amplitude has been normalized to the volume fraction ϕ_B of the bilayer decorating the minimal surface.

The numerical results confirm that the amplitudes can be described by eqs 14 and 15. Figure 8 contains the numerical results for three Bragg reflections—210, 322, and 420. The first two are prohibited by the $Im\bar{3}m$ symmetry group. The 210 is prohibited because if one of the indices is equal to zero the sum of the other two should be even. When two indices are equal (as in 322), the third one should be even. As we can see in Figure 8 the amplitudes for both 210 and 322 are symmetric in the interface surface displacement ξ. The amplitude of the 420 peak (allowed by the symmetry group of the base TPMS) is antisymmetric in ξ.

Table 2 contains the SFs, forms of the MFs and α correction parameters for the 33 most prominent Bragg
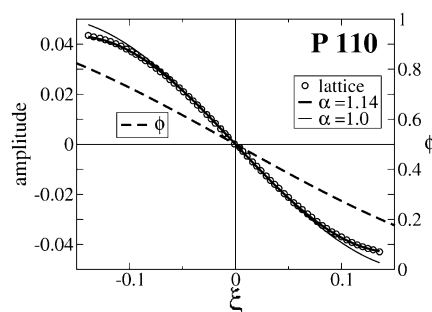
Figure 9. The 110 amplitude of the channel associated with the P TPMS. The circles give the numerical result. The thin solid line corresponds to the uncorrected isotropic fit ($\alpha = 1$). A good approximation of the dependence on the displacement *l* of the bounding interface PS is given by a corrected MF ($\alpha = 1.14$).
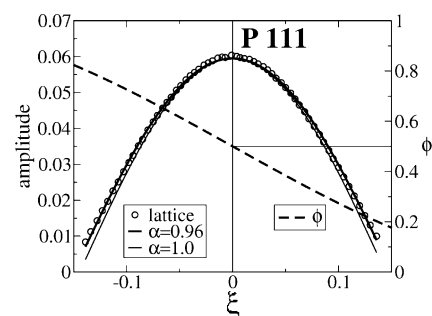
Figure 10. Caption analogous to Figure 9.

reflections arising from a network associated with the P TPMS. In a case of most of the chosen reflections the amplitude dependence on the displacement ξ is almost isotropic[41]—it does not require significant corrections ($\alpha \approx 1$). Still in case of few of the peaks the α correction parameters needed to fit the dependence differ from unity significantly. An example of this is given in Figures 9 and 10 for the 110 and 111 reflections, respectively.

4.2. The Schwartz D, Double Diamond Surface. The D—double diamond—TPMS has the $Pn\bar{3}m$ (no. 224) symmetry and each of the networks $Fd\bar{3}m$ (no. 227)[42] (see Figure 2). None of those groups are centrosymmetric. We have chosen an origin which results in purely real amplitudes allowed by the D TPMS symmetry ($Pn\bar{3}m$). This makes all the other amplitudes purely imaginary as is denoted in Table 3. The $Pn\bar{3}m$ symmetry group sets the following reflection conditions:

$$Pn\bar{3}m: \begin{cases} 0kl: & k+l=2n \\ h00: & h=2n \end{cases} \qquad (20)$$

However, the unit cell for the networks is linearly two times larger than that for the sole D TPMS. Therefore, we had to use the larger unit cell and the conditions (eq 20) have to be rewritten as follows:

$$Pn\bar{3}m: \begin{cases} hkl: & h, k, l = 2n \\ 0kl: & k+l = 4n \\ h00: & h = 4n \end{cases} \qquad (21)$$

Now it can be compared with the symmetry group of the networks ($Fd\bar{3}m$), which allows additionally

$$Fd\bar{3}m/Pn\bar{3}m: \begin{cases} hkl: & h+k, k+l, l+h = 2n \\ hhl: & h+l = 2n \end{cases} \qquad (22)$$

Thus, the nonzero amplitudes permitted only by (22)

Table 3. Scattering Data for the D TPMS Based Phases[a]

The Scattering Data for the **D** Multicontinuous Cubic Phases

hkl	M_{hkl}	F^S_{hkl}	F^M	α_{hkl}	hkl	M_{hkl}	F^S_{hkl}	F^M	α_{hkl}
0 0 0	1	0.5	ϕ		7 1 1	24	0.0041i	c	1
1 1 1	8	−0.1504i	c	0.98	6 4 2	48	0.1914	s	1
2 2 0	12	0.9588	s	1.08	5 5 3	24	−0.0095i	c	1
3 1 1	24	−0.0183i	c	0.96	7 3 1	48	0.0057i	c	1
2 2 2	8	0.9702	s	1	6 4 4	24	0.3723	s	1
4 0 0	6	−0.5233	s	1.09	6 6 0	12	0.3395	s	1
3 3 1	24	−0.0252i	c	0.98	5 5 5	8	−0.0090i	c	1
4 2 2	24	0.4241	s	1	6 6 2	24	0.3624	s	1
3 3 3	8	−0.0215i	c	0.98	7 5 3	48	−0.0036i	c	1
5 1 1	24	0.0106i	c	0.95	6 6 4	24	0.4188	s	1
4 4 0	12	0.5159	s	1	7 5 5	24	−0.0054i	c	1
5 3 1	48	−0.0037i	c	0.98	7 7 1	24	−0.0045i	c	1
4 4 2	24	0.5599	s	1	7 7 3	24	−0.0048i	c	1
6 2 0	24	−0.3769	s	1	9 5 1	48	0.0035i	c	1
5 3 3	24	−0.0095i	c	1	6 6 6	8	0.0044	s	1
4 4 4	8	0.5822	s	1	7 7 5	24	−0.0052i	c	1
5 5 1	24	−0.0089i	c	1					

[a] This footnote is the same as that for Table 2.
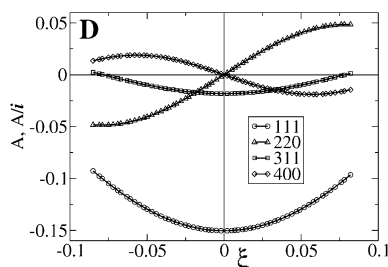
Figure 11. Amplitudes for the channels bounded by an interface PS associated with the double diamond TPMS. The 111 and 220 reflections are permitted by the symmetry of the base TPMS ($Pn\bar{3}m$) while the 311 and 400 peaks are allowed only by the lower group of the networks ($Fd\bar{3}m$). This results in a different form of the MF. The symbols show the numerical results while the solid lines present the fit through eq 15. See section 4.2 for a detailed description.

should be described by the symmetric MF (*cosine* form) and the ones allowed by (21) by the antisymmetric MF (*sinus* form). Figure 11 shows the amplitudes for the 111, 220, 311, and 400 reflections. For example the 111 reflection is permitted by the $Fd\bar{3}m$ symmetry ($1 + 1 = 2$) but not by the $Pn\bar{3}m$ symmetry ($1 \neq 2$).

4.3. The G Gyroid Surface. The G−gyroid−TPMS (Figure 2) belongs to the $Ia\bar{3}d$ symmetry group (no. 230) with the following reflection conditions:

$$Ia\bar{3}d: \begin{cases} hkl: \ h + k + l = 2n \\ 0kl: \ k,\, l = 2n \\ hhl: \ 2h + l = 4n \\ h00: \ h = 4n \end{cases} \quad (23)$$

The labyrinths created by the surfaces parallel to the G TPMS are of the $I4_132$ symmetry group (no. 214)[42] which allows a larger class of nonzero amplitudes:

$I4_132$:

$$\begin{cases} hkl: \ h + k + l = 2n \ \ \text{same as } Ia\bar{3}d \\ 0kl: \ k + l = 2n \ \ \text{as compared with } k,\, l = 2n \ (Ia\bar{3}d) \\ hhl: \ l = 2n \ \ \text{as compared with } 2h + l = 4n \ (Ia\bar{3}d) \\ h00: \ h = 4n \ \ \text{same as } (Ia\bar{3}d) \end{cases}$$
$$(24)$$

The $Ia\bar{3}d$ group is centrosymmetric, and if the contrast electron density would have the same symmetry as the

Table 4. Scattering Data for the G TPMS Based Phases[a]

The Scattering Data for the **G** Multicontinuous Cubic Phases

hkl	M_{hkl}	F^{hkl}_S	F^M	α_{hkl}	hkl	M_{hkl}	F^{hkl}_S	F^M	α_{hkl}
0 0 0	1	0.5	ϕ		4 3 3	24	−0.0109i	c	1
1 1 0	12	−0.1232i	c	0.98	5 3 0	24	0.0071i	c	1
2 1 1	24	0.6544	s	1.07	4 4 2	24	−0.0078i	c	1
2 2 0	12	0.4306	s	0.97	5 3 2	48	−0.0040i	c	1
3 1 0	24	0.0141i	c	0.98	5 3 2	48	−0.1114	s	1
2 2 2	8	−0.0297i	c	0.95	6 1 1	24	−0.2287	s	1
3 2 1	48	−0.0166i	c	1.04	5 4 1	48	−0.1652	s	1
3 2 1	48	−0.0971	s	1.05	6 3 1	48	−0.1992	s	1
4 0 0	6	−0.3375	s	1.04	4 4 4	8	0.4112	s	1
3 3 0	12	−0.0034i	c	1.13	5 4 3	48	0.3012	s	1
4 2 0	24	−0.3309	s	1	5 5 0	12	0.0041i	c	1
3 3 2	24	0.4751	s	1	6 4 2	48	0.0036i	c	1
4 2 2	24	0.2770	s	1	6 4 2	48	0.0741	s	1
4 3 1	48	0.0047i	c	0.96	6 5 3	48	−0.0751	s	1
4 3 1	48	0.1898	s	1	6 5 5	24	0.3112	s	1
5 1 0	24	0.0060i	c	1	6 6 4	24	0.2403	s	1
5 2 1	48	0.0041i	c	0.98	6 6 6	8	−0.0047i	c	1
5 2 1	48	−0.0737	s	1					

[a] The footnote is the same as that for Table 2.

G TPMS, the amplitudes could be phased to purely real values.[36] Here we have chosen an origin which sets the same relative phasing between the real parts of the amplitudes allowed by the TPMS symmetry as in the case of the bilayer structures.[36] Still this results in purely imaginary values of the peaks allowed only by the $I4_132$ group and, in few cases, also a nonzero imaginary component of the reflections permitted by $Ia\bar{3}d$. Thus, in the case of the 321, 431, 521, 532, and 642 peaks the amplitude for a single network of electron density ρ_0 has to be evaluated as follows:

$$A(\mathbf{q}, \rho_0, \xi_0) =$$
$$\rho_0\left(i\mathscr{T}\mathscr{F}^S \cos(q\alpha_{hkl}\xi_0) + \mathscr{R}\,\mathscr{F}^S\frac{\sin(q\alpha_{hkl}\xi_0)}{q\alpha_{hkl}} \right) \quad (25)$$

The imaginary ($\mathscr{T}\mathscr{F}^S$) and real ($\mathscr{R}\,\mathscr{F}^S$) parts of the structure factor for these peaks are listed in Table 4 together with the data for all the other 24 reflections.

5. Results for the I−WP TPMS Based MCTPS

The I-WP TPMS belongs to the $Im\bar{3}m$ symmetry group (the same as P−plumber's nightmare surface). Since the group is centrosymmetric, the origin has been chosen in such a way as to make all of the nonzero amplitudes purely real. The I-WP TPMS is not balanced, and the base minimal surface does not have a higher symmetry than the networks determined by the interface PSs. Therefore, there is no distinction between the reflections allowed by the symmetry of the base TPMS and that of the derived networks. It turns out that in terms of the amplitudes dependence on the PS displacement ξ the base TPMS ($\xi = 0$) does not possess a common significance. In other words the amplitudes can be fitted by a simple *cosine* form of the MF yet one has to introduce an additional parameter ξ_{hkl} by which the displacements have to be shifted. The ξ_{hkl} parameter is specific for each reflection. Then the MF for all of the reflections arising from a network possessing an interface associated with the I-WP TPMS reads as follows:

$$\mathscr{F}^M(\mathbf{q}, \xi) = \cos(q\alpha_{hkl}(\xi - \xi_{hkl})) \quad (26)$$

All of the parameters including the SFs have been fitted to the numerically obtained scattering amplitudes. The

**Table 5. Scattering Data for the I-WP TPMS Based Phases**

The Scattering Data for the **I−WP** Multicontinuous Cubic Phases

hkl	M_{hkl}	$F_{hkl}^{\mathcal{S}}$	α_{hkl}	ξ^*_{hkl}	hkl	M_{hkl}	$F_{hkl}^{\mathcal{S}}$	α_{hkl}	ξ^*_{hkl}
0 0 0	1	0.477			6 0 0	6	0.0145	1.48	0.0297
1 1 0	12	−0.1044	1.54	0.0262	6 1 1	24	0.0072	1.54	0.0206
2 0 0	6	0.1113	1.33	−0.0333	5 3 2	48	−0.0065	1.42	−0.0281
2 1 1	24	0.0137	1.89	−0.0232	6 2 0	24	0.0068	1.48	0.0081
2 2 0	12	−0.0330	1.30	0.0738	6 2 2	24	−0.0062	1.38	0.0374
3 1 0	24	0.0336	1.42	0.0697	6 3 1	48	0.0041	1.46	−0.0178
2 2 2	8	−0.0211	1.14	−0.0562	4 4 4	8	−0.0057	1.46	−0.0152
3 2 1	48	0.0051	1.16	−0.0481	7 1 0	24	−0.0085	1.48	−0.0052
4 0 0	6	−0.0313	1.46	0.0176	6 4 0	24	0.0053	1.53	−0.0040
4 1 1	24	−0.0117	1.53	0.0024	5 5 2	24	0.0056	1.45	0.0061
3 3 0	12	0.0197	1.39	−0.0095	7 3 0	24	−0.0056	1.48	−0.0270
4 2 0	24	−0.0134	1.41	−0.0235	7 3 2	48	0.0048	1.44	0.0050
3 3 2	24	−0.0077	1.37	0.0265	8 0 0	6	0.0087	1.47	−0.0262
4 2 2	24	0.0112	1.33	0.0102	8 2 0	24	−0.0043	1.48	0.0208
5 1 0	24	0.0153	1.51	−0.0286	7 5 2	48	−0.0040	1.44	0.0275
4 3 1	48	0.0044	1.51	0.0462	9 1 0	24	0.0055	1.49	0.0083
5 2 1	48	−0.0041	1.38	0.0216	9 3 2	48	−0.0039	1.45	0.0182
4 4 0	12	0.0078	1.48	0.0406	10 0 0	6	−0.0055	1.49	−0.0096
5 3 0	24	−0.0101	1.46	0.0259	10 4 0	24	0.0022	1.51	0.0225
4 4 2	24	−0.0064	1.39	0.0441	9 7 4	48	0.0020	1.50	−0.0155

[a] The MF has the same form for all of the reflections (see eq 34). Apart from the SFs and α correction parameters also the shifts $\xi^*_{hkl} = \xi_{hkl}/a$ of the displacement ξ are given. See section 5 for explanation.
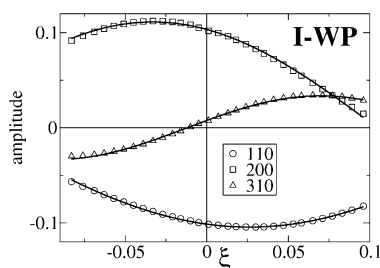
Figure 12. Scattering amplitudes for a channel associated with the I-WP TPMS. The MF given by eq 26 (solid lines) gives a very good agreement with the numerical results (symbols).
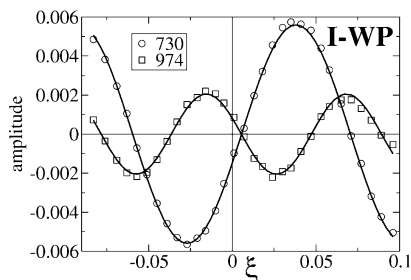
Figure 13. Higher order scattering amplitudes for a channel associated with the I-WP TPMS. Solid lines show the fit (eq 26) to the numerical results (symbols).

data are included in Table 5. Most of the chosen peaks display quite large deviations from the isotropic model[36,41]—the α correction parameters significantly differ from unity. Still the fits provide a very good approximation of the scattering amplitudes. The approximation works almost equally well for the peaks with small scattering vector (see Figure 12) and for the higher order reflections (Figure 13).

6. The General Solution

Lets now consider an arbitrary n-block copolymer molecule given by a set of the volume fractions $\{\phi_i\}$ and the corresponding electron densities $\{\rho_i\}$. Figure 7a−c shows a schematic illustration for a case with $n = 3$ blocks. Each of the interfaces defined by the displace-

ments $\xi_i(\tilde{\phi}_i)$ are parallel surfaces. For simplicity the density map is shifted by the electron density of the outermost block (Figure 7d). The electron density map can be expressed as a sum of the channels contained within the subsequent parallel surfaces. In other words, the electron density distribution within the unit cell is composed of n subspaces of volume fractions ϕ_i and electron densities ρ_i can be viewed as a sum of $(n − 1)$ single labyrinths with volume fractions equal to $\tilde{\phi}_i = \sum_{j=1}^{i} \phi_j$ and electron densities $\tilde{\rho}_i = \rho_i − \rho_{i+1}$. Then the amplitude for an arbitrary n-block copolymer system forming a n-continuous cubic phase can be written as

$$A(\mathbf{q}, \{\tilde{\phi}_i\}, \{\tilde{\rho}_i\}) = \mathscr{F}^S(\mathbf{q})\sum_{i=1}^{n-1} \tilde{\rho}_i \mathscr{F}^M(\mathbf{q}, \xi(\tilde{\phi}_i)) \quad (27)$$

The MF's are given by eq 15 and all the data needed to evaluate this expression for the most prominent Bragg reflections for the P, D, G and I− WP MCTPS are given in Tables 2−5.

The intensity of an *hkl* peak for a monocrystalline sample is

$$I_{hkl} = A(\mathbf{q}_{hkl}, \{\tilde{\phi}_i\}, \{\tilde{\rho}_i\}) A^*(\mathbf{q}_{hkl}, \{\tilde{\phi}_i\}, \{\tilde{\rho}_i\}) \quad (28)$$

In all the cases when the amplitude is purely real, it can be further simplified to $I = A^2$. For the powder samples each intensity (eq 28) should be multiplied by the multiplicity factor $\mathscr{M}_{hkl}$ which is also given in Tables 2−5.

7. Modeling the Interface Width

The structures formed in block copolymers can have sharp interfaces in a strong segregation regime or very diffuse interfaces in a weak segregation regime. The interface width should have an effect on the relative amplitudes of the scattering peaks. To include this effect into our model we have assumed an error function type of the interface.[43] This will enable us to use the electron density distribution of an ideally segregated system and convolute it with a Gaussian distribution. This is an analogue of the Debye−Waller factor, which in the case of amphiphilic mixtures takes into account the fluctua-
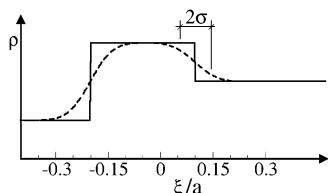
Figure 14. One-dimensional step electron density profile $\rho(\xi)$ is given by a solid line. After a convolution with a Gaussian distribution with the standard deviation σ we obtain a continuous electron density distribution (dashed line). The interface profiles between subsequent domains are given by an error function. The interface width d can be associated with twice the dispersion $d = 2\sigma$.

tions of the interface. We want to show in a very short way that in fact the interface width d will come into the equations analogously to the fluctuations amplitude in the model for bicontinuous cubic phases in lyotropic liquid crystals.[36]

Continuous electron density distributions $\bar{\rho}(\xi)$ with error function like interfaces profiles can be built from an ideally segregated step density distribution $\rho(\xi)$ by a convolution with a Gaussian distribution:

$$\bar{\rho}(\xi) = \frac{1}{\sqrt{2\pi}\sigma} \int_{-\infty}^{+\infty} d\xi' \, \rho(\xi') \exp\left[-(\xi - \xi')^2/2\sigma^2\right] \quad (29)$$

An example of a resulting profile $\bar{\rho}(\xi)$ is shown in Figure 14. The interface width d can be associated with twice the standard deviation σ. To recover the influence of the interface width on the scattering amplitude, we have to rewrite eq 27 in a continuous form:

$$A(\mathbf{q}, \bar{\rho}(\xi)) = \mathscr{F}^S(\mathbf{q}) \int_{-\infty}^{+\infty} d\xi \left(-\frac{d\bar{\rho}(\xi)}{d\xi}\right) \mathscr{F}^M(\xi) \quad (30)$$

Because $\bar{\rho}(\xi)$ is equal to zero in $-\infty$ and $+\infty$ we can rewrite (30) as

$$A(\mathbf{q}, \bar{\rho}(\xi)) = \mathscr{F}^S(\mathbf{q}) \int_{-\infty}^{+\infty} d\xi \bar{\rho}(\xi) \left(\frac{d\mathscr{F}^M(\xi)}{d\xi}\right) \quad (31)$$

The derivative of the MF is

$$\frac{d}{d\xi}\mathscr{F}^M(\xi) =$$
$$\begin{cases} \cos(\alpha_{hkl}q\xi) = [\exp(i\alpha_{hkl}q\xi) + \exp(-i\alpha_{hkl}q\xi)]/2 \\ -q\alpha_{hkl}\sin(\alpha_{hkl}q\xi) = q\alpha_{hkl}[\exp(-i\alpha_{hkl}q\xi) - \exp(i\alpha_{hkl}q\xi)]/2 \end{cases}$$
$$(32)$$

After insertion of (29) and (32) into (31) for each form of the MF, we have a sum of two integrals. Because of their similarity, we will discuss here only one of them:

$$a = \frac{\mathscr{F}^S}{\sqrt{2\pi}\sigma} \int_{-\infty}^{\infty} d\xi \rho(\xi) \int_{-\infty}^{\infty} d\xi' \exp[i\alpha_{hkl}q\xi]$$
$$\exp[-(\xi - \xi')^2/2\sigma^2] \quad (33)$$

which after few steps can be simplified to

$$a = \mathscr{F}^S[\int_{-\infty}^{\infty} d\xi \, \rho(\xi) \exp[iq\xi]] \exp\left[-\frac{1}{2}\alpha_{hkl}{}^2 q^2 \sigma^2\right] \quad (34)$$

The integrand in the brackets is exactly of the same form as the first part of the MF (eq 32). The whole dependence on the interface width is contained in the

last exponential term analogous to the Debye–Waller factor

$$\mathscr{F}^{DW} = \exp\left[-\frac{1}{2}\alpha_{hkl}{}^2 q^2 \sigma^2\right] \quad (35)$$

and the scattering amplitudes for a diblock copolymer bicontinuous cubic phase read

$$A(\mathbf{q}, \tilde{\phi}_1, \tilde{\rho}_1, d_{1,2}) = \mathscr{F}^S(\mathbf{q})\tilde{\rho}_1\mathscr{F}^M(\mathbf{q}, \xi(\tilde{\phi}_1))$$
$$\exp\left[-\frac{1}{8}\alpha_{hkl}{}^2 q^2 d^2{}_{1,2}\right] \quad (36)$$

where $d_{1,2}$ is the interface width between the first and second domain ($d_{1,2} = 2\sigma_{1,2}$). For multicontinuous phases, one can take into account different widths $d_{i,i+1}$ for each pair of blocks i and $i + 1$. Then the final relation for the scattering amplitude (eq 27) becomes

$$A(\mathbf{q}, \{\tilde{\phi}_i\}, \{\tilde{\rho}_i\}, \{d_{i,i+1}\}) = \mathscr{F}^S(\mathbf{q})\sum_{i=1}^{n-1}\tilde{\rho}_i\mathscr{F}^M(\mathbf{q}, \xi(\tilde{\phi}_i))$$
$$\exp\left[-\frac{1}{8}\alpha_{hkl}{}^2 q^2 d^2{}_{i,i+1}\right] \quad (37)$$

In our following article, we will discuss in detail how the information about the interface widths can be extracted from an experimental scattering pattern.

8. Summary

The model presented in this article allows evaluation of the scattering amplitudes for an arbitrary multi continuous cubic architecture based on either P, D, G, or I-WP TPMS. This should greatly facilitate a quantitative analysis of the scattering spectra of the n-block copolymer systems exhibiting three-dimensional order. In the following paper, the application of the method to various architectures will be given showing the typical X-ray scattering spectra obtained from the analytical formulas derived in this paper. Finally we note that the analysis presented in this paper encompasses as a special case the results given in our previous work on the X-ray spectra for the cubic phases formed in the low molecular weight surfactants mixed with water.[36,37]

References and Notes

(1) Bates, F. S.; Fredrickson G. H. *Annu. Rev. Phys. Chem.* **1990**, *41*, 525; Bates F. S. *Science* **1991**, *251*, 898.
(2) Leibler, L. *Macromolecules* **1980**, *13*, 1602.
(3) Fredrickson, G. H.; Helfand, E. *J. Chem. Phys.* **1987**, *87*, 697.
(4) Matsen, M. W.; Schick, M. *Phys. Rev. Lett.* **1994**, *72*, 2660.
(5) Matsen, M. W.; Schick, M. *Macromolecules* **1994**, *27*, 4014.
(6) Matsen, M. W.; Schick, M. *Curr. Opin. Colloid Interface Sci.* **1996**, *1*, 329.
(7) Matsen, M. W.; Bates, F. S. *Macromolecules* **1996**, *29*, 1091.
(8) Aksimentiev, A.; Hołyst, R. *J. Chem. Phys.* **1999**, *111*, 2329.
(9) The existence of the close-packed sphere phase is a theoretical prediction. As noted by one of the reviewers the experiments indicate that the long-range order in this phase is destroyed by fluctuations; see for example: Sakamoto, N.; Hashimoto, T.; Han, C. D.; Kim, D.; Vaidya, N. Y. *Macromolecules* **1997**, *30*, 1621.
(10) Molau, G. E. *Block Copolymers*; Aggarawal, S. L., Ed.; Plenum Press: New York, 1970.

(11) Thomas, E. L.; et al. *Macromolecules* **1986**, *19*, 2197. Herman D. S.; et al. *Macromolecules* **1987**, *20*, 2940.

(12) Hasegawa, H.; et al. *Macromolecules* **1987**, *20*, 1651.

(13) Thomas, E. L.; et al. *Nature (London)* **1988**, *334*, 598.

(14) Hajduk, D. A.; Harper, P. E.; Gruner, S. M.; Honeker, C. C.; Kim, G.; Thomas, E. L.; Fetters, L. J. *Macromolecules* **1995**, *28*, 2570.

(15) Hajduk, D. A.; Harper, P. E.; Gruner, S. M.; Honeker, C. C.; Kim, G.; Thomas, E. L.; Fetters, L. J. *Macromolecules* **1994**, *27*, 4063.

(16) Schulz, M. F.; Bates, F. S.; Almdal, K.; Mortensen, K. *Phys. Rev. Lett.* **1994**, *73*, 86.

(17) Stadler, R.; et al. *Macromolecules* **1995**, *28*, 3080.

(18) Hamley, I. W. *The physics of block copolymers*; Oxford University Press: New York, 1998.

(19) Spontak, R. J.; et al. *Macromolecules* **1996**, *29*, 4494.

(20) Schulz, M. F.; et al. *Macromolecules* **1996**, *29*, 2857.

(21) Hanley, K. J.; Lodge, T. P.; Huang, C. I. *Macromolecules* **2000**, *33*, 5918.

(22) Seki, M.; Suzuki, J.; Matsushita, Y. *J. Appl. Cryst.* **2000**, *33*, 285.

(23) Wang, C. Y.; Lodge, T. P. *Macromol. Rapid Commun.* **2002**, *23*, 49.

(24) Ren, Y.; Lodge, T. P.; Hillmyer, M. A. *Macromolecules* **2002**, *35*, 3889.

(25) Lodge, T. P.; Pudil, B.; Hanley, K. J. *Macromolecules* **2002**, *35*, 4707.

(26) Floudas, G.; et al. *Macromolecules* **2001**, *34*, 2947.

(27) Finnefrock, A. C.; et al. *Angew. Chem. Int. Ed.* **2001**, *40*, 1208.

(28) Anderson, D. M.; Davies, H. T.; Scriven, L. E.; Nitsche, J. C. C. *Adv. Chem. Phys.* **1990**, *77*, 337−396.

(29) Anderson, D.; Wennerström, H.; Olsson, U. *J. Phys. Chem.* **1989**, *93*, 4243.

(30) The calculations have been performed on the TPMS obtained by a minimization of the Landau−Ginzburg scalar potential in the real space.[31.]

(31) Góźdź, W. T.; Hołyst, R. *Phys. Rev. E* **1996**, *54*, 5012−5029.

(32) There is yet another family of interfaces called level surfaces (LS). (Wohlgemuth, M.; Yufa, N.; Hoffman, J.; Thomas, E. L. *Macromolecules* **2001**, *34*, 6083) that can be used for modeling the channels in multicontinuous cubic architectures. Such surfaces are given by the equation $F(x, y, z) = $ const. The properties of the level surfaces can be determined once the function $F(x, y, z)$ is specified. By the proper choice of the function $F(x, y, z)$ we can obtain level surfaces which are very close to CMC surfaces (in particular minimal surfaces). In principle one could find a function $F(x, y, z)$ such that the level surfaces could be very close to PS surfaces. Therefore the general definition of LS provides an easy route towards various surfaces of a given symmetry. Still the exact shape of the surfaces does not have to reflect the physical interfaces in block copolymer cubic phases. Moreover the exact shape of the surface does not influence strongly the X-ray scattering pattern.

(33) Harper, P. E.; Gruner, S. M. *Eur. Phys. J. E* **2000**, *2*, 217−228.

(34) Harper, P. E.; Gruner, S. M.; Lewis, R. N. A. H.; McElhaney, R. N. *Eur. Phys. J. E* **2000**, *2*, 229−245.

(35) Garstecki, P.; Hołyst, R. *J. Chem. Phys.* **2000**, *113*, 3772−3779.

(36) Garstecki, P.; Hołyst, R. *Langmuir* **2002**, *18*, 2519.

(37) Garstecki, P.; Hołyst, R. *Langmuir* **2002**, *18*, 2529.

(38) Babin, V.; Garstecki, P.; Hołyst, R. *Phys. Rev. B* **2002**, *66*, 235120.

(39) The equation relating volume fraction of the black channel with the normalized displacement ξ_1^* by which the interface PS is defined follows from the equation on the bilayer volume fraction.[29] The bilayer contained between two PS symmetrically displaced from the base minimal surface (by ξ_1^* and $-\xi_1^*$) has a volume fraction $\phi_B = 2s_0^* \xi_1^* + 4/3 \, \pi\chi\xi_1^{*3.}$ Then the volume fraction of the *minus* channel is the volume fraction of the channel defined by the base minimal surface (ϕ_-) plus/minus the volume between the minimal surface and the shifted interface. The latter is simply half the bilayer volume fraction and hence eq 2.

(40) Mackay, A. L. *Nature (London)* **1985**, *314*, 604−606.

(41) Clerc, M.; Dubois-Violette, E. *J. Phys. II* **1994**, *4*, 275−286.

(42) *International Tables For Crystalography*.

(43) Usually the interface density profiles are modeled with hyperbolic tangent function.[44] This can be very well approximated by the error function.

(44) Stamm, M. *Macromol. Symp.* **1996**, *112*, 25.